

# Monolithic Mesophase Silica with Large Ordering Domains

N. A. Melosh,<sup>†,§</sup> P. Davidson,<sup>‡</sup> and B. F. Chmelka<sup>\*,†</sup>

Contribution from the Departments of Chemical Engineering and Materials, University of California, Santa Barbara, California 93106, and Laboratoire de Physique des Solides, Bat. 510, Université Paris-Sud, 91405 Orsay Cedex, France

Received August 5, 1999

**Abstract:** Two-dimensional X-ray diffraction (XRD) analyses of transparent mesoscopically ordered silica/block copolymer composite monoliths reveal single-crystal-like patterns that correspond to well-ordered hexagonal domains that are greater than 1 cm × 1 mm × 1 mm in size. Analyses of the diffraction patterns reveal highly uniform hexagonal domains with narrow distributions of orientational order that are characterized by a  $\phi$ -mosaic smaller than 2° in the plane of the hexagonal lattice and a  $\chi$ -mosaic smaller than 11° along the cylindrical aggregate axes. XRD and TEM results also show that the composite monoliths have large well-ordered cubic mesophase domains in the meniscus regions of the samples. Boundaries between the hexagonal and cubic domains in the monoliths reflect gradual transitions between the two epitaxially related structures. Such large single-domain hexagonal and cubic mesostructures were furthermore preserved following removal of the organic species by calcination to produce mesoporous silica monoliths.

## Introduction

Progress in the development of new synthesis and processing strategies for preparing mesoscopically ordered inorganic mesoporous materials, such as the MCM and SBA families of mesoporous oxides,<sup>1,2</sup> is leading to new levels of design and control over material compositions and structures. Initially, these materials were synthesized as powders suitable for catalytic and separation applications with a variety of ordered mesophase architectures, including hexagonal, lamellar, and cubic structures. Since then, efforts to improve the processability of these materials have led to low-molecular-weight surfactant/inorganic mesophase composites or mesoporous solids in the form of films,<sup>3–7</sup> spheres,<sup>8–10</sup> and orientationally ordered solids.<sup>11–13</sup>

Several authors have reported aligned silica–surfactant mesostructures in thin films produced at various interfaces;<sup>13–17</sup> in addition, Ryoo et al.<sup>4</sup> have produced thick mesoporous films with uniform birefringence, though the degree of alignment was not further characterized. Generally, materials with such macroscopic morphologies have tended to have diminished mesoscopic ordering, reduced thermal stability, and/or small domain sizes, which constrain their utility for a number of applications, particularly in optics.

Substantial processing advantages have been demonstrated, and larger mesoscopic ordering length scales achieved, by using amphiphilic block copolymers as structure-directing agents for network-forming inorganic species, instead of low-molecular-weight surfactants. For example, silica/block copolymer materials have been synthesized with high degrees of mesoscopic order in a variety of macroscopic morphologies, including powders,<sup>2</sup> films,<sup>18</sup> fibers,<sup>19</sup> and monoliths.<sup>20–23</sup> Using a combination of polymer and sol–gel processing techniques, films or fibers can be prepared with high degrees of orientational order.<sup>18,19</sup> This has created opportunities for a variety of new applications where molecular-level alignment and organization may provide enhanced material or device properties, such as in lasers or

\* To whom correspondence should be addressed.

<sup>†</sup> Department of Chemical Engineering, University of California.

<sup>§</sup> Department of Materials, University of California.

<sup>‡</sup> Université Paris-Sud.

(1) Kresge, C. T.; Leonowicz, M. E.; Roth, W. J.; Vartuli, J. C.; Beck, J. S. *Nature* **1992**, 359, 710–712.

(2) Zhao, D.; Feng, J.; Huo, Q.; Melosh, N.; Fredrickson, G. H.; Chmelka, B. F.; Stucky, G. D. *Science* **1998**, 279, 548–552.

(3) Ogawa, M.; Igarashi, T.; Kuroda, K. *Bull. Chem. Soc. Jpn.* **1997**, 70, 2833–2837.

(4) Ryoo, R.; Ko, C. H.; Cho, S. J.; Kim, J. M. *J. Phys. Chem. B* **1997**, 101, 10610–10613.

(5) Lu, Y.; Gangull, R.; Drewien, C. A.; Anderson, M. T.; Brinker, C. J.; Gong, W.; Guo, Y.; Soye, H.; Dunn, B.; Huang, M. H.; Zink, J. I. *Nature* **1997**, 389, 364–368.

(6) Attard, G. S.; Bartlett, P. N.; Coleman, N. R. B.; Elliot, J. M.; Owen, J. R.; Wang, J. H. *Science* **1997**, 278, 838–840.

(7) Whitehead, A. H.; Elliot, J. M.; Owen, J. R.; Attard, G. S. *Chem. Commun.* **1999**, Feb 21, 331–332.

(8) Grün, M.; Lauer, I.; Unger, K. K. *Adv. Mater.* **1997**, 9, 254–257.

(9) Huo, Q.; Feng, J. L.; Schüth, F.; Stucky, G. D. *Chem. Mater.* **1997**, 9, 14–17.

(10) Lu, Y. F.; Fan, H. Y.; Stump, A.; Ward, T. L.; Rieker, T.; Brinker, C. J. *Nature* **1999**, 398, 223–226.

(11) Firouzi, A.; Schaefer, D. J.; Tolbert, S. H.; Stucky, G. D.; Chmelka, B. F. *J. Am. Chem. Soc.* **1997**, 119, 9466–9477.

(12) Tolbert, S. H.; Firouzi, A.; Stucky, G. D.; Chmelka, B. F. *Science* **1997**, 278, 264–268.

(13) Raimondi, M. E.; Maschmeyer, T.; Templer, R. H.; Seddon, J. M. *Chem. Commun.* **1997**, 19, 1843–1844.

(14) Schacht, S.; Huo, Q.; Voigt-Martin, I. G.; Stucky, G. D.; Schüth, F. *Science* **1996**, 273, 768–771.

(15) Yang, H.; Coombs, N.; Sokolov, I.; Ozin, G. A. *Nature* **1996**, 381, 589–592.

(16) Yang, H.; Kuperman, A.; Coombs, N.; Mamiche-Afara, S.; Ozin, G. A. *Nature* **1996**, 379, 703–705.

(17) Miyata, H.; Kuroda, K. *Chem. Mater.* **1999**, 11, 1609–1614.

(18) Zhao, D.; Yang, P.; Melosh, N.; Feng, J.; Chmelka, B. F.; Stucky, G. D. *Adv. Mater.* **1998**, 10, 1380.

(19) Yang, P.; Zhao, D.; Chmelka, B. F.; Stucky, G. D. *Chem. Mater.* **1998**, 10, 2033–2036.

(20) Bagshaw, S. A.; Prouzet, E.; Pinnavaia, T. J. *Science* **1995**, 269, 1242–1244.

(21) Templin, M.; Franck, A.; Du Chesne, A.; Leist, H.; Zhang, Y.; Ulrich, R.; Schädler, V.; Wiesner, U. *Science* **1997**, 278, 1795–1798.

(22) Göltner, C. G.; Henke, S.; Weissenberger, M. C.; Antonietti, M. *Angew. Chem., Int. Ed.* **1998**, 37, 613–616.

(23) Melosh, N. A.; Lipic, P.; Bates, F. S.; Wudl, F.; Stucky, G. D.; Fredrickson, G. H.; Chmelka, B. F. *Macromolecules* **1999**, 32, 4332–4342.

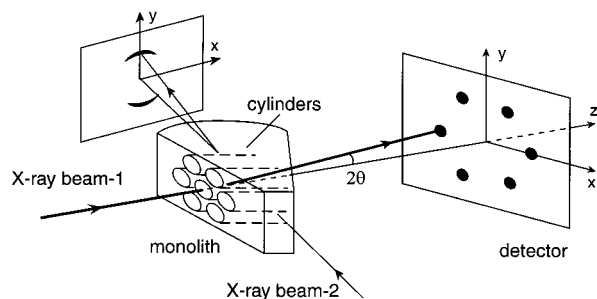


**Figure 1.** Schematic diagram of the X-ray and sample configurations, with the cylindrical aggregates (not drawn to scale) within the composite aligned parallel (beam 1) or perpendicular (beam 2) to the incident X-rays.

nonlinear optical media. However, the preparation of such mesoscopically organized inorganic/organic composites or mesoporous solids as transparent bulk materials with large domain sizes, as often found in liquid crystalline systems, has not previously been achieved. We report here, for the first time, the synthesis and characterization of transparent silica/block copolymer monoliths with large (>1 cm) oriented single hexagonal and cubic mesostructured domains, which are preserved after calcination to yield opaque mesoporous silica monoliths.

### Experimental Section

Transparent block copolymer/silica monoliths were synthesized in an acidic silica sol–gel solution containing nonionic poly(ethylene oxide)–poly(propylene oxide)–poly(ethylene oxide) (PEO–PPO–PEO) amphiphilic block copolymer species as structure-directing agents. The specific conditions used for the samples studied here were as follows:<sup>24</sup> 0.542 g of Pluronic F127 (EO<sub>106</sub>PO<sub>70</sub>EO<sub>106</sub>, BASF USA, Mount Olive, NJ) was added to a solution of 1.4 mL of <sup>2</sup>HCl (pH 1.5) and 5.0 mL of ethanol-*d* (CH<sub>3</sub>CH<sub>2</sub>O<sup>2</sup>H), and the solution was stirred until the block copolymer had completely dissolved. The amount of block copolymer could be varied from 0.5 to 1.0 g, depending upon processing conditions, and produced results similar to those of the sample examined here. While the solution was still being stirred, 2.0 mL of tetraethoxysilane (TEOS, Aldrich Chemicals) was added, forming a homogeneous mixture in approximately 10 min. The solution was then transferred to a 30-mL poly(propylene) vial and sealed tightly for 12 h. The vial lid was then removed until gelation of the sol solution occurred (3–4 days), after which the vial was resealed. The sealed samples were subsequently allowed to age at room temperature for 6 weeks. At the end of this period, the products had shrunk ~20% in diameter yet retained the shape of their containers. The samples were uncovered and stored at room temperature to allow excess solvent to evaporate, resulting in 1–2-mm-thick, 2.5-cm-diameter transparent disks.

Two-dimensional (2D) X-ray diffraction (XRD) studies were performed with the X-ray beam delivered by a copper rotating anode generator and punctually focused by two perpendicular mirrors, as described elsewhere.<sup>25</sup> The scattered X-rays were detected either on imaging plates or on photographic films for better resolution. The experimental setup is illustrated schematically in Figure 1 for the two X-ray beam configurations used: one in which the X-ray beam was directed parallel to the principal axes of the cylindrical aggregates and the other with the beam sent normal to the cylinder axes.

Transmission electron microscopy (TEM) images were taken with a JEOL 2010 electron microscope operating at 200 keV. Samples were prepared by grinding pieces of the composites into powders and depositing the powders on amorphous carbon-coated copper grids for analysis.

(24) These synthetic conditions are similar to those reported in ref 23; however, the ethanol concentration was doubled, and deuterated solvents were used for future NMR studies.

(25) Impéror-Clerc, M.; Davidson, P. *Eur. Phys. J. B* **1999**, *19*, 93–104.

### Results and Discussion

Transparent silica/block copolymer composite monoliths and opaque mesoporous silica monoliths were synthesized with high degrees of mesoscopic order in large aligned domains. Long-range, single-crystal-like mesostructural organization and macroscopic orientational order in the samples were established using 2D X-ray diffraction and TEM. Such large domain sizes with very narrow distributions of orientational order ( $\langle P_2 \rangle = 0.99$  for the hexagonal phase) have not previously been observed in inorganic/organic or mesoporous monoliths.

**Large Single-Domain Hexagonal Mesostructures.** Two-dimensional X-ray diffraction patterns are shown in Figure 2 for a single 1.5-cm × 1-mm × 1-mm domain taken from a 50 wt % EO<sub>106</sub>PO<sub>70</sub>EO<sub>106</sub>/SiO<sub>2</sub> monolith. The patterns in Figure 2 are from the same region of the same sample but were acquired with different orientations of the X-ray beam, as illustrated schematically in Figure 1. For the 2D XRD pattern shown in Figure 2a, the X-ray beam was directed parallel to the principal axes of the hexagonally arranged cylindrical aggregates within the domain, yielding a 6-fold hexagonal spot pattern. The pattern displays six intense (10) reflections with 6-fold symmetry, characteristic of the two-dimensional hexagonal lattice. In addition, several higher order (11) and (20) reflections are observed at  $\sqrt{3}$  and 2 times the scattering vector modulus of the (10) reflection, confirming the hexagonal assignment (similar to SBA-15 materials<sup>2</sup>). The lattice parameter for this hexagonal structure was calculated to be  $a = 129.4$  Å, based on the  $d_{100}$  spacings of 111.9 Å. The six-spot hexagonal diffraction pattern in Figure 2a is representative of others acquired when the X-ray beam was directed through the plane of the sample disk, indicating that the cylindrical aggregates lie lengthwise within the plane of the disk, parallel to the air–sample interface.

Whereas polycrystalline materials yield circular 2D X-ray diffraction lines, the sharply resolved Bragg diffraction spots in Figure 2 indicate that the silica/EO<sub>106</sub>PO<sub>70</sub>EO<sub>106</sub> sample is composed of a single hexagonal domain over the sample volume probed by the X-ray beam, ~1 mm<sup>3</sup>. The overall size of such a highly aligned domain can be established by translating the sample piece through the X-ray beam and monitoring the constancy of the diffraction pattern. The hexagonal domain, whose diffraction pattern is featured in Figure 2, extended throughout the entire 1.5-cm × 1-mm × 1-mm volume of the piece cut from the monolith; identical diffraction patterns were produced at all points over this single piece. No additional spots or rotation of the pattern were observed, indicating a mesoscopically homogeneous single-crystal-like domain at least 1.5 cm long. Analyses of other sample pieces revealed highly aligned domains with similar length scales, typically ~0.5 cm<sup>2</sup> × 1 mm. To our knowledge, such large orientationally ordered domains obtained without shearing or other means of alignment have not previously been produced in inorganic–organic composites or mesoporous solids and are uncommon in liquid crystal systems as well.<sup>26</sup> Their appearance here is attributed to the slow annealing process employed to produce these monoliths, which is discussed in more detail below.

The widths of the X-ray diffraction spots obtained from a single hexagonal domain allow the ordering of the cylindrical aggregates to be assessed. For an ideal hexagonal mesophase, the cylinders would be arranged on a perfect hexagonal lattice, resulting in an X-ray diffraction pattern consisting of sharp spots with resolution-limited widths. Deviations from this ideal situation are manifested by broadening of the XRD reflections.

(26) Malthête, J.; Davidson, P. *Bull. Soc. Chim. Fr.* **1994**, *131*, 812–815.

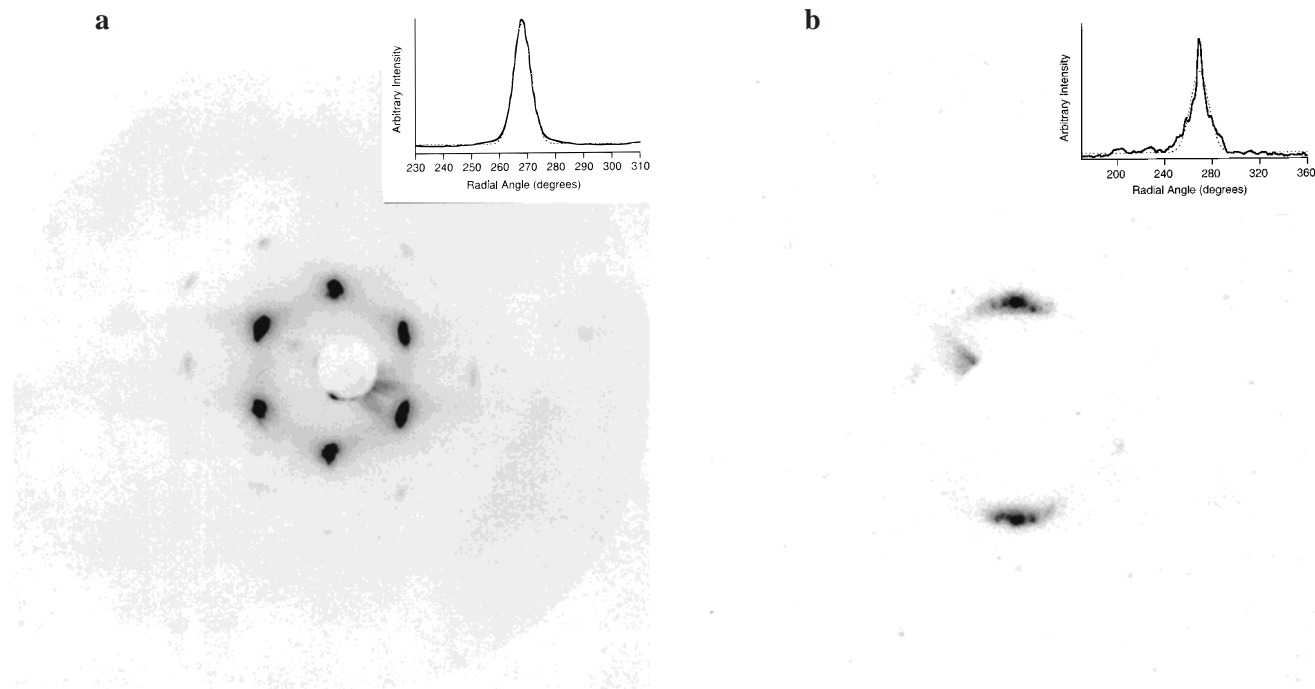


**Figure 2.** Two-dimensional (2D) X-ray diffraction patterns of an as-synthesized 50 wt %  $\text{EO}_{106}\text{PO}_{70}\text{EO}_{106}$  block copolymer/silica composite acquired with the X-ray beam aligned (a) along and (b) perpendicular to the 6-fold symmetry axis of a single-crystal-like hexagonal domain. Well-resolved Bragg diffraction spots indicate that long-range ordering extends throughout the 1-mm<sup>3</sup> sample volume probed by the X-ray beam. In (a), the (10) spacing is measured to be 111.9 Å, with a fwhm of 2° for the primary reflections. Higher order (11) and (20) reflections can also be observed, indicative of a highly periodic mesostructure. The insets in (a) and (b) display the azimuthal radial intensity distributions of one of the (10) reflections and the Gaussian curve fits used to calculate the  $\phi$ -mosaic (fwhm = 2°) and  $\chi$ -mosaic (fwhm = 11°), respectively.

Broadening in the radial direction (i.e., from the reflection to the center of reciprocal space) is due either to a small domain size or to a gradual loss of the positional correlations of the hexagonal ordering. Broadening of the reflections into arcs along tangential directions (i.e., in planes perpendicular to the corresponding radial directions) is due to a distribution of cylindrical aggregate orientations in the aligned hexagonal domain.<sup>27–29</sup> The degree of orientational order is then characterized by the full-width-at-half-maximum (fwhm) values of the intensity distributions of the (10) diffraction spots in each of these orthogonal directions, known as the “ $\phi$ -mosaic” and “ $\chi$ -mosaic”, respectively; narrower widths indicate higher degrees of orientational order.<sup>29</sup> Such widths and their corresponding orientation distributions can be established from Gaussian fits to the (10) peak shapes, as plotted, for example, in the insets of Figure 2. Numerical estimates of the mosaics were corrected for finite beam-size effects, measured to be 5° for the experimental configuration used.

The hexagonal reflections shown in Figure 2a are limited in the radial direction by the 1000-Å instrumental resolution of the measurement, indicating that the hexagonal positional order extends over at least this length scale. Typical (10) reflection widths measured in the tangential direction were 2–3° fwhm ( $\phi$ -mosaic) for hexagonal domains obtained from as-synthesized silica/ $\text{EO}_{106}\text{PO}_{70}\text{EO}_{106}$  monoliths. Such values establish that the cylindrical aggregates are arranged into a nearly perfect hexagonal array, with average distributions of alignment of  $\pm 1^\circ$  over the 1-mm<sup>3</sup> sample volume probed by the X-ray beam.

These well-defined Bragg reflections result from very small deviations in the arrangements and alignments of the cylindrical aggregates from perfect hexagonal symmetry.

Of particular interest for the hexagonal structure are the continuity and orientational ordering of the cylindrical aggregates along the director axis. Due to the small sizes of mesoscopically ordered powder particles or domains present in most inorganic/organic samples investigated in the literature, cylinder lengths longer than several micrometers have not previously been demonstrated. However, from the large single hexagonal domains present within the silica/ $\text{EO}_{106}\text{PO}_{70}\text{EO}_{106}$  composites, aggregate lengths larger than 1 cm are measured. For a perfectly ordered system, the cylindrical aggregates would lie straight and align parallel to each other. Consequently, an X-ray beam directed perpendicular to such an array would produce an XRD pattern consisting of two primary spots oriented perpendicular to the cylinder axes. Deviations of cylinder orientations away from perfect longitudinal alignment will produce broadening of the XRD pattern features, as measured from the fwhm ( $\chi$ -mosaic) of the primary two-spot XRD reflections.<sup>29</sup> Figure 2b shows the XRD pattern obtained for the same single-domain piece used in Figure 2a, but with the X-ray beam aimed perpendicular to the cylindrical aggregate axes (see Figure 1). The pattern in Figure 2b displays two intense narrow reflections with a fwhm ( $\chi$ -mosaic) of 11°, corresponding to an order parameter of  $\langle P_2 \rangle = 0.99$ , determined by fitting a Gaussian curve to the broader (lower) reflection. The vertical orientation and narrowness of the two-spot pattern establishes that, in real space, the cylindrical aggregates are highly aligned and that, over the volume probed ( $\sim 1 \text{ mm}^3$ ), the average distribution of longitudinal cylinder orientations is less than  $\pm 6^\circ$  from parallel alignment. Correlating the cylinder orientational ordering with the macroscopic location of the hexagonal domain in the monolith, furthermore, establishes that the aggregates are

(27) Pople, J. A.; Hamley, I. W.; Fairclough, J. P. A.; Ryan, A. J.; Booth, C. *Macromolecules* **1998**, *31*, 2952–2956.

(28) Guinier, A. *X-ray Diffraction in Crystals, Imperfect Crystals and Amorphous Bodies*; Dover: New York, 1994.

(29) Davidson, P.; Clerc, M.; Ghosh, S. S.; Maliszewskyj, N. C.; Heiney, P. A.; Hynes, J., Jr; Smith, A. B., III. *J. Phys. II (France)* **1995**, *5*, 249–262.



**Figure 3.** 2D XRD pattern obtained from a hexagonally ordered mesoporous silica structure following calcination. The sample configuration is the same as in Figure 2a, yielding (10), (11), (20), (21), and (30) reflections. The sharp diffraction spots and higher order peaks indicate that the structure is predominantly a highly ordered single domain. The lattice constant is 107.7 Å, and the inset displays the azimuthal radial intensity distribution of the (10) reflections, which indicates a  $\phi$ -mosaic of  $\text{fwhm} = 8^\circ$ . A small amount of cubic impurity is also present.

aligned parallel to the air-sample interface of the monolithic disk. These measurements indicate a higher degree of orientational order than has been produced in other bulk inorganic/organic systems,<sup>12</sup> or by shearing Pluronic block copolymers,<sup>27,30–33</sup> which usually produces  $\chi$ -mosaics of  $\sim 20$ – $30^\circ$ . The high degree of orientational ordering is comparable to that of highly aligned liquid crystal systems.<sup>25</sup>

After calcination, pieces cut from the monolith retain their macroscopic shapes and well-ordered hexagonal mesostructures, though transparency is lost due to microcracking within the silica matrix. Several as-synthesized pieces with large single hexagonal domains ( $\sim 0.5 \text{ cm} \times 2 \text{ mm} \times 1 \text{ mm}$ ) were calcined at  $450^\circ \text{C}$  in air, yielding sharp XRD patterns, such as that shown in Figure 3. The sharp hexagonal spot pattern observed for the primary (10) reflections reveals that a high degree of hexagonal mesostructural ordering and long-range alignment have been preserved within the calcined single domain. Substantial shrinkage of the mesostructured silica framework is observed following calcination, with the (10) reflection measured to be 93.3 Å (reduced from 111.9 Å in the as-synthesized sample), corresponding to a lattice parameter of  $a = 107.7 \text{ Å}$  (reduced from 129.4 Å). Despite this 17% contraction of the lattice constant, the hexagonal ordering of the cylindrical array remains remarkably good, with the  $\text{fwhm}$  ( $\phi$ -mosaic) of the primary (10) reflections measured to be  $8^\circ$ . In addition, the higher order (11),

(20), and (21) peaks become more intense. This is attributed to the greater electron density contrast between the silica walls and the open mesopore channels, which causes the samples to scatter the incident X-rays more strongly after removal of the structure-directing block copolymer species. The  $\phi$ -mosaic of the calcined hexagonal mesoporous silica domain is larger than that measured for the composite precursor domain ( $\text{fwhm} = 2^\circ$ , Figure 2a), indicating somewhat diminished orientational order within the calcined sample.

Additional structural information on deformations and defect structures in the calcined mesophase silica domain can be obtained from the diffuse scattering and locations of higher-order Bragg reflections in the 2D XRD pattern in Figure 3. Straight diffuse lines extending between the individual (10) reflections form a diffuse hexagon that is visible in Figure 3 and more weakly so in Figure 2a. Such lines have previously been observed in X-ray scattering patterns of hexagonal mesophases of low-molar-mass thermotropic mesogens and have been interpreted as arising from localized defects, such as dislocations of the hexagonal lattice.<sup>34</sup> More noticeably, two additional rows of weak reflections are present in the scattering patterns (most clearly seen along the vertical axis) of Figure 3, which were also observed prior to calcination. These reflections do not belong to the hexagonal lattice but appear to correspond to an oriented epitaxially related mesostructure. We believe that these additional reflections arise from a small amount (roughly a few percent from the relative XRD intensities) of another ordered mesostructure, possibly cubic (see below). Bragg reflection intensities and TEM images also demonstrate a slight distortion of the hexagonal ordering, due to preferential thickening of the silica walls along the dense (10) plane axes. Indeed, significant differences exist among the relative intensities of the six (10) spots, as shown in the inset of Figure 3: the two reflections at  $0^\circ$  and  $180^\circ$  are much more intense than the other four. Rotation of the sample within the beam lessened the intensity differences but did not eliminate them. From the diffraction pattern alone, however, it is difficult to judge with certainty whether the intensity distribution arises from a significant structural feature or may be due to misalignment of the sample within the X-ray beam.

To complement the structural analysis provided by XRD, the calcined single hexagonal domain was powdered and analyzed also by TEM. Figure 4 shows a representative micrograph of the hexagonal structure observed throughout this sample, similar to that observed in hexagonal SBA-15 materials<sup>2</sup>. Along with the well-ordered honeycomb structures, areas of reduced order are also visible in the lower right corner of the image, appearing as modulated “cylinder/layer” structures. In these regions, the silica walls separating the cylindrical channels have thickened preferentially along the hexagonal (10) planes, producing a structure that appears as hexagonally spaced pores interspersed with silica lamellae. Similar thickening of the hydrophilic regions has been observed in hexagonal-to-cubic-to-lamellar phase transformations in liquid crystal systems, where the denser planes in the hexagonal structure become the layers of the lamellar structure.<sup>35</sup> The periodicity and hexagonal arrangement of the channels are unaffected, so that the diffraction pattern(s) from these regions coincide with that of the bulk hexagonal phase, though the thicker (10) walls lead to greater scattering intensity normal to the plane(s). As the diffraction pattern of a purely lamellar structure consists of two (10) spots aligned normal to the layers, the fact that the thicker silica walls in some

(30) Schmidt, G.; Richtering, W.; Lindner, P.; Alexandridis, P. *Macromolecules* **1998**, *31*, 2293–2298.

(31) Hamley, I. W.; Koppi, K. A.; Rosedale, J. H.; Bates, F. S.; Almdal, K.; Mortensen, K. *Macromolecules* **1993**, *26*, 5959–5970.

(32) Bates, F. S.; Koppi, K. A.; Tirrell, M.; Almdal, K.; Mortensen, K. *Macromolecules* **1994**, *27*, 5934–5936.

(33) Pople, J. A.; Hamley, I. W.; Fairclough, J. P. A.; Ryan, A. J.; Komanschek, B. U.; Gleason, A. J.; Yu, G. E.; Booth, C. *Macromolecules* **1997**, *30*, 5721–5728.

(34) Levelut, A. M. *J. Phys. Lett. (France)* **1979**, *40*, L81.

(35) Clerc, M.; Levelut, A. M.; Sadoc, J. F. *J. Phys. II (France)* **1991**, *1*, 1263–1276.

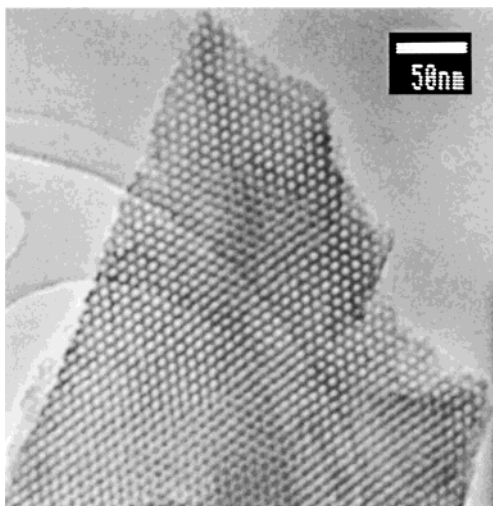


**Figure 4.** Representative transmission electron microscopy (TEM) image from the same calcined sample used in Figure 3. Uniform hexagonal mesoscopic ordering is observed over large regions of the sample. The preferential thickening of some of the silica layers between the hexagonally packed cylinders visible in the lower right of the image shows the deformation responsible for the two significantly more intense XRD reflections visible in Figure 3.

regions of the sample have a degree of lamellar character is consistent with the increased intensities of the  $0^\circ$  and  $180^\circ$  (10) reflections (Figure 3, inset). Furthermore, correlating the XRD intensity distribution with the macroscopic orientation of the domain within the original monolith establishes that these thicker (10) planes are uniformly parallel to the air–sample interface. These modulated cylinder/layer regions are believed to result from block copolymer and/or solvent concentration gradients near a phase boundary, with the resultant structures kinetically trapped by the polymerizing silica network.

**Large Mesostructured Cubic Domains.** Near the outer edges of the transparent as-synthesized disk monoliths, large single domains are found with high degrees of cubic mesostructural ordering. Such cubic domains, both in as-synthesized composites and in calcined mesoporous solids, yield highly resolved 2D XRD spot patterns, such as those shown in Figure 5. These each display four intense (100) spots, along with several (110) and (200) reflections at higher angles. The clear 4-fold symmetry and  $1:1/\sqrt{2}:1/2$   $d$ -spacing of the reflections identify the structures as cubic. This was confirmed by rotating the samples  $90^\circ$  in the X-ray beam and observing an identical diffraction pattern, corresponding to the existence of three mutually orthogonal 4-fold symmetry axes. From Figure 5a, the lattice spacing of the as-synthesized cubic mesostructured domains was measured to be  $a = 97 \text{ \AA}$ , substantially smaller than the spacing observed for the hexagonal domains found in the bulk region of the same as-synthesized composite monolith. However, the  $\phi$ -mosaic of the cubic lattice was similar, with a (100) fwhm of less than  $3^\circ$  (as shown from the radial intensity distribution plot in the inset of Figure 5a), characteristic of a highly periodic, single cubic mesophase domain with high structural fidelity over distances of  $\sim 1\text{--}2 \text{ mm}$ .

Calcination of the composite cubic domains yielded mesoporous cubic silica with comparable mesoscopic ordering and macroscopic morphologies. 2D XRD analyses indicate that high degrees of mesostructural order and alignment are preserved in the calcined cubic products. As determined from Figure 5b, the cubic (100)  $d$ -spacing shrank 4% to  $93.1 \text{ \AA}$ , and the fwhm of these reflections broadened only slightly to  $4^\circ$ . The higher order (110), (200), and (210) reflections also increased in intensity,

consistent with increased electron density contrast created by removing the organic moieties from the pores. A representative TEM micrograph obtained from the calcined cubic material is displayed in Figure 6, showing a highly periodic cubic array of  $\sim 30\text{-\AA}$  spherical pores with  $\sim 40\text{-\AA}$ -thick silica matrix. (The TEM images provide only approximate estimates of pore size, as the structures have been observed to shrink under the electron beam. In addition, the fracture surface imaged may not be at the midplane of the pores or the sample may be tilted with respect to the electron beam, so that the actual pore sizes associated with the TEM image of Figure 6 may be larger.)

Translation of the X-ray beam across a large piece of the as-synthesized monolith revealed that the cubic domains are located along the outer rim of the disk monolith and are also present in a thin ( $<0.1 \text{ mm}$ ) layer at the air–sample interface. The cubic mesophase is believed to form in regions of the macroscopic monolith that experience faster solvent evaporation and silica polymerization rates, namely near the air–monolith interfaces. Scanning the X-ray beam radially from the edge of the disk into the bulk center revealed well-defined cubic scattering patterns for  $1\text{--}2 \text{ mm}$ , followed by patterns indicating a mixed-phase cubic/hexagonal zone  $\sim 1 \text{ mm}$  thick and a purely hexagonal region in the monolith center thereafter. Within the mixed-phase regions, the hexagonal and cubic mesophases were epitaxially related, with the hexagonal cylinder director axes in registry with the cubic (111) direction, consistent with previous studies of cubic/hexagonal phase transitions.<sup>35</sup> Along the most highly curved meniscus regions, the cubic diffraction pattern (not shown here) was distorted, characterized by a 2-fold symmetry axis, broader  $d_{100}$  line widths, and non-Gaussian intensity distributions. This reduced ordering is attributed to the large gradients in solvent concentration that are expected to exist near the air–monolith surface, which lead to spatially varying rates of block copolymer self-assembly, structural annealing, and silica polymerization.

The epitaxial relationship between the cubic and hexagonal mesophase domains provides important insight into the formation and evolution of these nonequilibrium structures. Previous studies of the phase behavior of amphiphilic  $\text{EO}_{106}\text{PO}_{70}\text{EO}_{106}$  in mixed water/oil solutions<sup>36</sup> have shown that the cubic phase is favored at lower concentrations of block copolymer (20–60 wt % to water) and hydrophobic additives ( $<10 \text{ wt } \%$  1-butanol or *p*-xylene). Above these concentrations, lamellar or hexagonal structures are favored. For the conditions considered here, the phase/synthesis space is substantially more complicated, because of the multicomponent, and particularly nonequilibrium (drying, self-assembling, polymerizing), characteristics of the monolith system. Nevertheless, the presence of hydrophilic solvents (water and ethanol) and oligomeric silica at the beginning of the synthesis reduce the concentration of the structure-directing  $\text{EO}_{106}\text{PO}_{70}\text{EO}_{106}$  species to roughly 7 wt % of the total solution, favoring formation of a cubic or disordered mesophase; this is supported by the lack of birefringence of the initial bulk composite sols. Due to the higher rate of solvent evaporation near the surface of the monolith compared to the bulk, it is probable that the cubic mesophase forms first near the air–sample interface by the relatively rapid polymerization of the silica, which solidifies the cubic composite mesostructure. This is consistent with separate mesostructured silica thin-film syntheses<sup>18</sup> using the same  $\text{EO}_{106}\text{PO}_{70}\text{EO}_{106}$  block copolymer structure-directing agent, which produced cubic structures under rapid drying conditions similar to those produced at the upper

(36) Holmqvist, P.; Alexandridis, P.; Lindman, B. *Macromolecules* **1997**, *30*, 6788–6797.

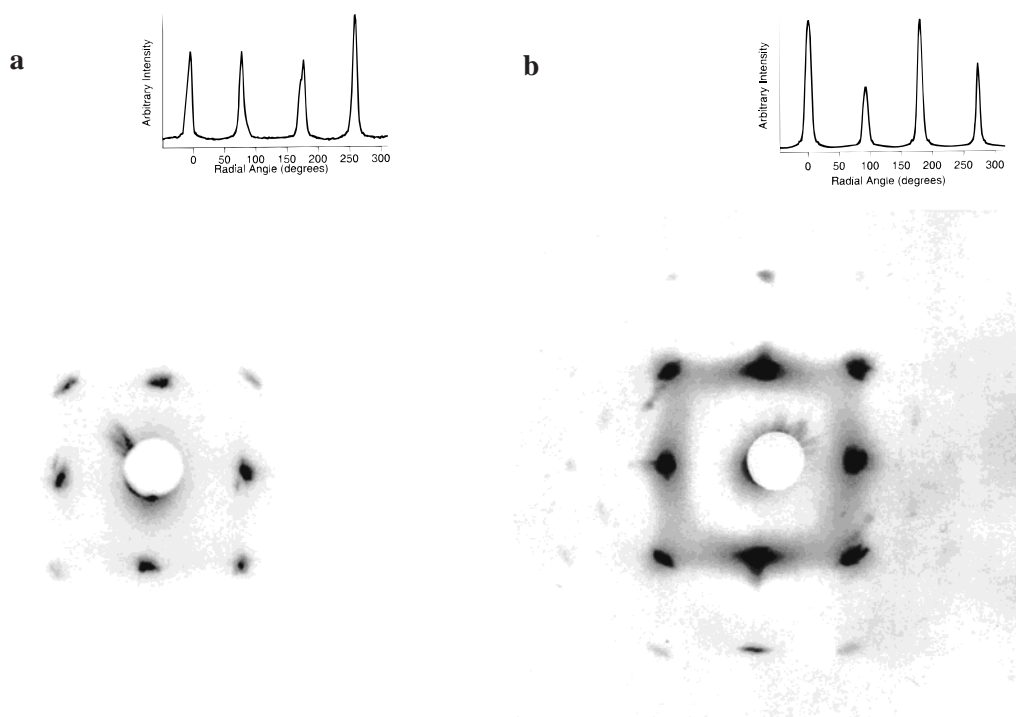


**Figure 5.** 2D XRD patterns of the cubic domains obtained from the meniscus region of a 50 wt % EO<sub>106</sub>PO<sub>70</sub>EO<sub>106</sub>/silica composites: (a) as-synthesized and (b) calcined. The sharp reflections indicate uniform long-range cubic mesostructural ordering, characterized by  $d_{100} = 97.0$  Å and fwhm = 3° for the as-synthesized sample, and  $d_{100} = 93.1$  Å and fwhm = 4° for the calcined material. Azimuthal radial intensity distributions of the (100) reflections are shown in the insets, indicating the high uniformity of the cubic ordering in these samples.

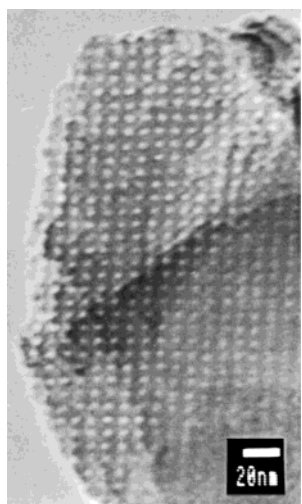


**Figure 6.** Representative TEM image from the same calcined cubic sample as used in Figure 5b. The structure appears to be composed of spherical pores (~30 Å in diameter) arranged on a cubic lattice; shrinkage of the material under the electron beam precludes definitive quantitative determination of feature dimensions. The cubic lattice appears to be slightly rectangular due to imperfect alignment with respect to the incident electron beam; the cubic symmetry is unambiguously established by X-ray diffraction (see Figure 5b).

meniscus of the bulk samples. In the interior of the monolith, slow transport of the water and ethanol solvents to the evaporation surface causes the system to cross gradually into the hexagonal region of the multicomponent phase/synthesis-space diagram. As this takes place, nucleation and growth of hexagonal mesostructures occur at, and emanate from, the (111) cubic direction into the bulk regions of the monolith. Slow cross-linking of the silica allows large oriented hexagonal EO<sub>106</sub>PO<sub>70</sub>EO<sub>106</sub> mesophase domains to form and thereby organize the silica network before it becomes too rigid to permit further

annealing or structural adjustments. The slow rates of the evaporation and polymerization processes allow the composites to anneal into large highly ordered and aligned hexagonal (or cubic) mesophase domains. More rapid evaporation of the solvent or polymerization of the silica (e.g., under more acidic conditions or at higher temperatures) resulted in poorly ordered mesophase monoliths and smaller domain sizes.

The epitaxial relationship and orientations of the cubic and hexagonal mesophases support initial formation of the cubic structure, followed by the appearance of cylindrical aggregates that are oriented with respect to both the interfacial cubic structure and the surfaces of the bulk monolith composite. The kinetic mechanisms and nonequilibrium processes that are responsible for the organization of the silica/block copolymer mesophases into such large highly ordered domains are currently under detailed investigation in our laboratories.

## Conclusions

Use of nonionic block copolymer structure-directing agents at high concentrations and under acidic pH conditions allows transparent silica/EO<sub>106</sub>PO<sub>70</sub>EO<sub>106</sub> block copolymer monoliths to be prepared with large single-domain hexagonal and cubic mesostructures. 2D X-ray analyses reveal these domains to be much more highly orientationally ordered than other organic–inorganic composite materials and comparable to well-aligned liquid crystal systems, with  $\phi$ -mosaics of 2–8° and  $\chi$ -mosaics of ~10°. A cubic mesophase was present along the edges and meniscus of the monolith examined; the interior of the bulk composite consisted of large hexagonal domains, in which the cylindrical axes were aligned parallel to the external monolith surface. Such structures arise because of interrelated nonequilibrium solvent evaporation, block copolymer self-assembly, and silica polymerization processes. Strategies based on these insights are expected to permit improved design and control of

the architecture and macroscopic orientation of mesoscopically ordered materials, with positive implications for optical and separations applications, where bulk anisotropy may be beneficial.

**Acknowledgment.** The authors thank Prof. G. D. Stucky and A. Freites for helpful discussions and BASF for the donation of the F127 block copolymer. This work was supported in part by the U.S. National Science Foundation through Grant CTS-

9871970 and the U.S. Army Research Office under Grant DAAH04-96-1-0443. XRD experiments were conducted at the Université de Paris-Sud using travel assistance provided by the U.S. NSF Division of International Programs under Grant INT-9726744. TEM measurements were conducted using central facilities of the NSF-supported UCSB Materials Research Laboratory under Award DMR-9632716.

JA992801B